Direct photonic–plasmonic coupling and routing in single nanowires

Ruoxue Yan, Peter Pausauskie, Jiaxing Huang, and Peidong Yang[1]

Department of Chemistry, University of California, Materials Sciences Division, Lawrence Berkeley National Laboratory, Berkeley, CA 94720

Edited by Mark A. Ratner, Northwestern University, Evanston, IL, and approved October 20, 2009 (received for review February 25, 2009)

Metallic nanoscale structures are capable of supporting surface plasmon polaritons (SPPs), propagating collective electron oscillations with tight spatial confinement at the metal surface. SPPs represent one of the most promising structures to beat the diffraction limit imposed by conventional dielectric optics. Ag nanowires have drawn increasing research attention due to 2D sub-100 nm mode confinement and lower losses as compared with fabricated metal structures. However, rational and versatile integration of Ag nanowires with other active and passive optical components, as well as Ag nanowire based optical routing networks, has yet to be achieved. Here, we demonstrate that SPPs can be excited simply by contacting a silver nanowire with a SnO_2 nanoribbon that serves both as an unpolarized light source and a dielectric waveguide. The efficient coupling makes it possible to measure the propagation-distance-dependent waveguide spectra and frequency-dependent propagation length on a single Ag nanowire. Furthermore, we have demonstrated prototypical photonic-plasmonic routing devices, which are essential for incorporating low-loss Ag nanowire waveguides as practical components into high-capacity photonic circuits.

waveguides | subwavelength | Ag nanowires | SnO_2 nanoribbons | propagation length

Recent research efforts have scaled down the plasmonic waveguides (1–6) from microscale metal stripes (7) to nanoparticles arrays (8, 9) and nanowires (4–6, 10–12), demonstrating the feasibility of subwavelength plasmonic optics. However, the inherent metal loss makes it impractical to transfer digital data across the entire photonic integrated circuit (IC) chip (≈1 mm) solely with plasmonic waveguides. It becomes increasingly important to be able to integrate plasmonic modules with low-loss, dielectric optical interconnects. To achieve such hybrid plasmonic-photonic circuit, it is critical to develop nanoscale plasmonic waveguides with reduced losses and small mode volume, and equally important, to ensure the compatibility with conventional optical circuitry. In this context, chemically-synthesized Ag nanowires have emerged as promising candidates for subwavelength plasmonic waveguides. The high crystallinity and atomically smooth surface of Ag nanowires should reduce the total propagation loss as compared with those microfabricated polycrystalline Ag waveguides. As a result, Ag nanowires are able to support surface plasmon propagation with 2D subwavelength mode confinement. However, integrating the low-loss Ag nanowire waveguides into a plasmonic-photonic routing network requires a simple, efficient, and versatile strategy to couple the light field in and out of the Ag nanowire so that the digital information can be launched and harvested.

The major challenge in optically excited surface plasmon polaritons (SPPs) in Ag nanowires lies in the dispersion relation mismatch for SPPs and photons. To bridge the difference in the wave vector k_x along the propagation direction $\hat{x}$, at any given photon energy $\hbar\omega$, the photon momentum $\hbar k_x$ ($= \hbar\omega/c\ \sqrt{\varepsilon_0}$, ε_0 being the dielectric constant of the dielectric enviroment) has to increase by a $\hbar\Delta k_x$ to couple photons into SPPs. Various methods have been proposed to bridge this gap and launch propagating SPPs in Ag nanowires. The total internal reflection (TIR) illumination method uses a prism to match the momentum of SPPs and the incident photons (5, 12). Direct local excitation was demonstrated by focusing a laser on the end facets of the Ag nanowires (6) or on a metallic nanoparticle attaching to the surface of the Ag nanowire that acts as a scattering center (13). A quantum emitter in the near-field of a Ag nanowire can excite propagating SPPs as the optical dipolar near-field contains large momentum components matching those of SPPs (14, 15). However, these coupling schemes do not lead to easy interconnection with conventional optical components for photonic IC fabrication. The recently reported polymer-Ag coupling method is an important advance toward on-chip integration. However, it still has many restrictions on the coupling conditions, including Ag nanowire orientation, position, and incident light field polarization (16).

Here, we propose a simple approach to couple SPPs into the Ag nanowires with an inorganic dielectric nano-waveguide, SnO_2 nanoribbon. Single-crystalline SnO_2 nanoribbon have been established as efficient UV-near (N)IR waveguides (17–19). Their high aspect ratio, strength, and flexibility enable their manipulation on surfaces, and can be assembled into optical networks and components. SnO_2 nanoribbons also exhibit photoluminescence with UV excitation and can act as a simultaneous nanoscale light source and waveguide. The Ag nanowires used in this work was synthesized by a modified polyol synthesis. The nanowires have five-fold twinning planes along their axis, and they are bound by five atomically smooth single crystalline {100} surfaces. We demonstrate that Ag nanowire SPPs can be excited by simply contacting with a SnO_2 nanoribbon with minimum restriction on the coupling conditions. SPPs can be launched into the Ag nanowire at arbitrary positions at any orientation. The assembly of the metal-dielectric junction is completely reversible, making it possible to monitor the properties of a single Ag nanowire while varying the interconnection and propagation condition. This versatile coupling strategy represents a major step toward realizing photonic-plasmonic hybrid circuitry, and has made possible the systematic far-field study on the SPP propagation in Ag nanowires.

Results and Discussion

Fig. 1*A* illustrates schematically the device setup. A silver nanowire sits on top of a SnO_2 nanoribbon waveguide that bridges two oxidized Si substrates. A UV laser was focused on the lower right corner of a SnO_2 nanoribbon to excite the broad-band photoluminescence (PL) of SnO_2, which is then waveguided along the nanoribbon toward the Ag nanowire. At the metal-dielectric boundary, photons traveling in the SnO_2 waveguide are scattered with a broad distribution of wave vectors and offer the Δk_x needed to match the momentum of photons

Author contributions: R.Y. and P.Y. designed research; R.Y., P.P., and J.H. performed research; P.Y. contributed new reagents/analytic tools; R.Y. and P.Y. analyzed data; and R.Y., P.P., J.H., and P.Y. wrote the paper.

The authors declare no conflict of interest.

This article is a PNAS Direct Submission.

[1]To whom correspondence should be addressed. E-mail: p_yang@berkeley.edu.

This article contains supporting information online at www.pnas.org/cgi/content/full/0902064106/DCSupplemental.

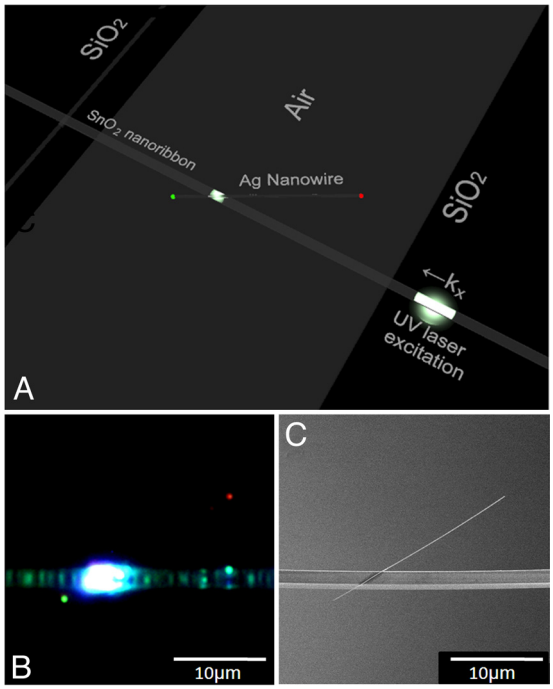

Fig. 1. Excitation and propagation of plasmon modes in a Ag nanowire waveguide. (*A*) A 3D schematic representation of the photonic-plasmonic routing device showing a Ag nanowire/SnO_2 nanoribbon cross-junction structure suspended between two SiO_2/Si wafers. A UV laser beam was focused on the lower right part of the SnO_2 nanoribbon to excite broad band PL. The PL is then waveguided along the nanoribbon to the metal-dielectric junction. Light scattered at junction was coupled into surface plasmon modes of the Ag nanowire, which then propagate along the wire and finally scattered back into free space photon at the two distal ends. (*B*) Optical microscope image showing the waveguiding of the SnO_2 PL in the actual photonic-plasmonic routing device illustrated in *A*. The large bright spot is the metal-dielectric junction where the photons in the SnO_2 nanoribbon couple into SPPs of the Ag nanowire waveguide. The emission (green and red) from both tips of the Ag nanowire can be observed by eye. The SnO_2 nanoribbon was excited from the far right section (data not shown). (*C*) SEM image of the same device in *B*.

and SPPs. The SPPs are guided within the 100-nm Ag nanowires and scatter back into free space photons at the distal ends of the wire. Fig. 1*B* is a microscope PL image of the real device built according to the schematics in Fig. 1*A*. A SnO_2 ribbon ($n = 2.1$) rests horizontally in the image, bridging a trench between two Si substrates (data not shown) with 500 nm thermal oxide ($n = 1.45$). The bright white PL of the nanoribbon was excited from the far right end of the ribbon with a 325 nm He:Cd laser, and while the photons are waveguided along the ribbon, they scattered off the local defects and other scatter centers, outlining the profile of the ribbon in the PL image. The bright white scattering spot is the metal-dielectric junction and the end emissions from the 20-μm long, 100-nm diameter Ag nanowire appearing in the image as a green spot on the lower left and a red spot on the upper right side of the ribbon. Both the Ag nanowire and the SnO_2 ribbon were positioned with a triple-axis micromanipulator equipped with a tungsten probe under a dark-field microscope. The SEM image of the device is shown in Fig. 1*C*.

The coupling between the SnO_2 nanoribbon and the Ag nanowire was observed regardless of their relative positions and orientations; however, the coupling efficiency depends heavily on the coupling angle, which is defined as the angle between the propagation directions of SPPs in the metal nanowire and photons in the original dielectric waveguide. Fig. S1 *a–d* shows the waveguiding images of a Ag nanowire with different coupling angles (labeled on the images) to the SnO_2 nanoribbon. The two sets of images were from the same Ag nanowire and SnO_2 nanoribbon. The distance of propagation from the coupling point to the distal end of the Ag nanowire were also kept the same so that propagation losses are the same and the intensity of the Ag nanowire end emissions can be directly compared as a measure of the energy input into the Ag nanowire. With a smaller the coupling angle (22°), more energy was coupled nonradiatively into the Ag nanowire, resulting in a brighter distal end emission; whereas with a large coupling angle (90°), the majority of energy coming out from the SnO_2 ribbon at the junction was lost by scattering into free space.

Although the absolute coupling efficiency between the SnO_2 nanoribbon and the Ag nanowire is difficult to measure, the relative coupling efficiency (η_c), which is defined here as the ratio between the total light input into the Ag nanowire ($I_{in,Ag}$) and the total light output from the SnO_2 (I_{out,SnO_2}) at the Ag-SnO_2 junction, can be estimated from the intensity of the Ag nanowire end emission and the radiative coupling loss resulting from the scattering at the wire-ribbon junction (for details, see *SI Materials and Methods*). Fig. S1*d* shows the angular dependence of photonic-plasmonic coupling efficiency at 980 nm. Here, η_c is largely dependent on the coupling angle. Smaller coupling angle favors the coupling of the photons in the dielectric waveguide into SPPs in the Ag nanowire with a smaller scattering loss, resulting in a higher η_c. This is true for all three wavelengths (532, 650, and 980 nm) that we tested.

The anglular dependence of coupling efficiency can be understood in terms of photonic-plasmonic mode matching. As we have discussed, at a given frequency ω, the momentum of the SPPs ($\hbar k_{SPP,x}$) in Ag nanowire is always larger than the momentum of the photon ($\hbar k_x$) in the dielectric waveguide along the SPP propagation direction x. In order for the photons to couple into SPPs, a certain mechanism has to exist to provide the extra momentum to bridge this gap. At small coupling angles (θ) where the momentum of photonic modes in the dielectric waveguide along the SPP propagation direction are large and better matched to the plasmonic modes, better coupling efficiency can be achieved. As the coupling angle increases, it would be more difficult for the photons to obtain the large extra Δk_x needed to couple into SPPs. In addition, the photonic-plasmonic coupling efficiency is also frequency-dependent. The estimated η_c for 20° coupling angle is 56% for 980-nm input photons, 43% for 650 nm, and 15% for 532 nm. Similar to the angular dependence, the frequency dependence of coupling efficiency is also related to momentum matching.

When squeezing the propagating SPPs into a highly-confined geometry like a 100-nm Ag nanowire, one central question is how the SPP propagation properties are modified compared with the bulk and other less confined geometries. One phenomenon that has been well-known for metal films (20) and metal microstripes (21) is a frequency-dependent propagation loss. The attenuation of the electromagnetic field along the propagation direction arises from two sources: the radiative and nonradiative loss. The radiative loss is attributed to back-coupling of SPPs into photons, and is characteristic for asymmetric two-interface systems, as with TIR coupled devices (20). Nonradiative loss, however, is due to absorption within the metal owing to the finite conductance of metal at optical frequencies. This nonradiative loss is the dominant contribution to our system where the Ag nanowire is in a symmetric dielectric environment. The nonradiative loss depends on the dielectric function of the oscillation frequency of the SPPs. As the frequency of the incident photon decreases from visible to the NIR, the real part of the Ag dielectric constant [$\mathrm{Re}\{\varepsilon_{Ag}\}<0$] becomes more negative, whereas the imaginary part $\mathrm{Im}\{\varepsilon_{Ag}\}$ remains approximately constant. As a result, the electromagnetic field decays faster inside the metal, thus less metal absorption or Joule heating is expected.

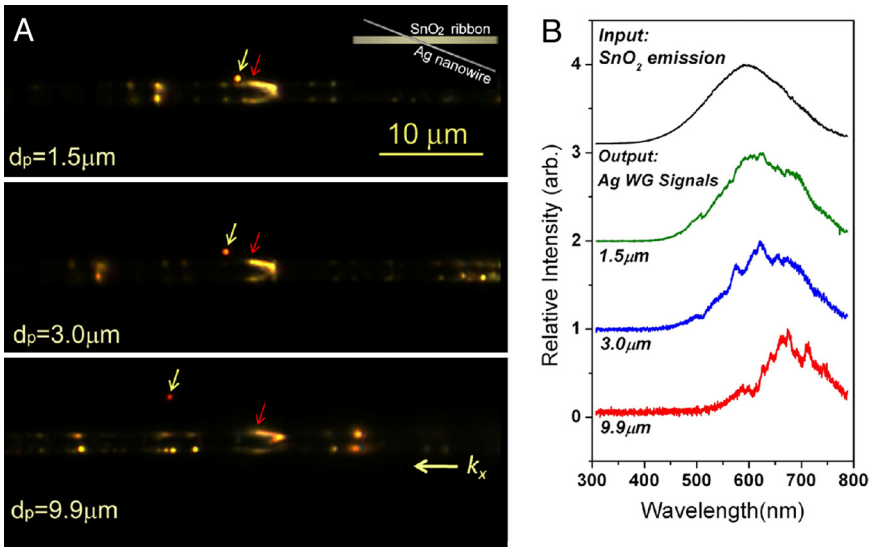

Fig. 2. Dependence of Ag nanowire waveguide spectra on the propagation distance (d_p). (*A*) True-color optical microscope images showing Ag nanowire/SnO_2 nanoribbon junctions of different propagating distance fabricated by micromanipulation. The coupling angle of the Ag/SnO_2 junction was kept constant, so that the coupling efficiency would be the same for all three images. The yellow arrow in each image points to the distal end emission point of the Ag nanowires, whereas the red arrow points to the starting point of the SPPs propagation. The distance in between the yellow and red arrows in each image is the actual distance of propagation d_p. The color of the end emission from the Ag nanowire contained more red-components with increasing d_p. The schematic representation of the setup is shown in the *Inset*. (*B*) Emission spectra of the Ag nanowire corresponding to the images in *A*, and the PL spectrum of the SnO_2 ribbon (input signal, excited with low laser power) used in the experiment.

For the Ag nanowires studied here, the frequency dependence of SPP propagation loss is clearly observed, as indicated by the color difference in the end emissions from the Ag nanowire in Fig. 1*B*. As the distance of SPP propagation (d_p), defined here by the distance between the silver wire tips and the coupling point on the SnO_2 ribbon, increases, the high-frequency components damp faster than the low frequency ones, so the frequency distribution of the SPPs is expected to red-shift with increasing d_p. Here, the left silver end-facet is just 3 μm from the SnO_2 ribbon, whereas the right end-facet is >10 μm from the SPP launching point, thus more red-components are expected from the right emission end-facet, as observed in the experiment.

To further confirm the frequency dependence of the propagation loss in Ag nanowires, we measured the tip emission spectra from a single Ag nanowire as a function of d_p and compared them with the SnO_2 ribbon emission, which serves as the input signal. Using the triple-axis micromanipulator, we were able to pick the Ag nanowire up from the SnO_2 ribbon, move it along the original orientation of the Ag nanowire, and put it back on the SnO_2 ribbon, so that different segments of the Ag nanowire came in contact with the SnO_2 waveguide. The true-color image of the device (Fig. 2*A*) and corresponding spectrum of the tip emission (Fig. 2*B*) were recorded at each position. Great care was taken to make sure that d_p was the only variable in the setup with the orientation of the Ag nanowire unchanged when the Ag nanowire was moved to a new position. Also, the particular position on the SnO_2 ribbon used for coupling was chosen to be free from large scattering centers that would increase background scattering signals.

The color images (collected with a 60× Olympus objective and a true-color camera) in Fig. 2*A* show a gradual change in the Ag nanowire tip emission colors from yellow, which is very close to the PL of the particular ribbon used here, to orange, and finally red when the distance of propagation, d_p, from the coupling point to the wire tip increased from 1.5 to 3.0 and 9.9 μm. Fig. 2*B* compares the spectra of both the SnO_2 ribbon PL emission, which is the input signal, to the tip emission spectra corresponding to the images in Fig. 2*A*. The input PL spectra taken from the tip of the SnO_2 ribbon was a smooth Gaussian peak extend from 400 to 800 nm and with the maximum at 590 nm. The tip emission spectrum for the lowest d_p = 1.5 μm resembles the input spectrum generally, but already starts to show a steep slope at the high-frequency side of the peak, a red-shift of the left intensity-cutoff wavelength to 430 nm, as well as a slight red-shift of the peak position, indicating an attenuation at the high-frequency end. The red shift of the peak position was more prominent for the tip spectra for longer d_ps, with the emission maximum at ≈620 nm for d_p = 3.0 μm, and ≈670m for d_p = 9.9 μm. The red-shift of the intensity-cutoff wavelength on the high-frequency side was also significant at these longer d_ps. For d_p = 3.0 μm, the intensity-cutoff was at ≈440 nm and was at ≈510 nm for d_p = 9.9 μm, a red-shift of >100 nm compared with the input spectrum. All these signs clearly demonstrate a much smaller propagation loss as the frequency decreases.

In a metal waveguide, the internal damping of SPP propagating away from the excitation along the propagation direction, $\bar{x}$, decreases exponentially as $I = I_0\, e^{-x/L}$. L, the propagation length, is defined by the characteristic length after which the intensity decreases to 1/e and is a measure of the propagation loss at a given frequency. L is determined by the imaginary part of the complex plasmon wave vector k_x, given by $L = \frac{1}{2Im\{k_x\}}$. To quantitatively measure the propagation length in our Ag nanowires, we designed an experimental setup illustrated in Fig. 3*A*. Similar to the coupling device used before, a SnO_2 nanoribbon was used to excite the SPP propagation in the Ag nanowire, but here, the input signal was no longer the broadband PL of SnO_2. Fixed to the tapered tip of an optical fiber coupled to the visible and NIR lasers, a SnO_2 nanoribbon served as a dielectric waveguide to deliver laser photons to the Ag nanowire. This probe made of a SnO_2 nanoribbon and an optical fiber was then mounted on a micromanipulator with a ≈15° angle to the focus plane of a dark-field microscope and is capable of scanning in three directions with 0.1-μm resolution. Fig. S1*a* shows a dark field image of the probe when the tip of the SnO_2 nanoribbon was brought into focus. This probe was then brought

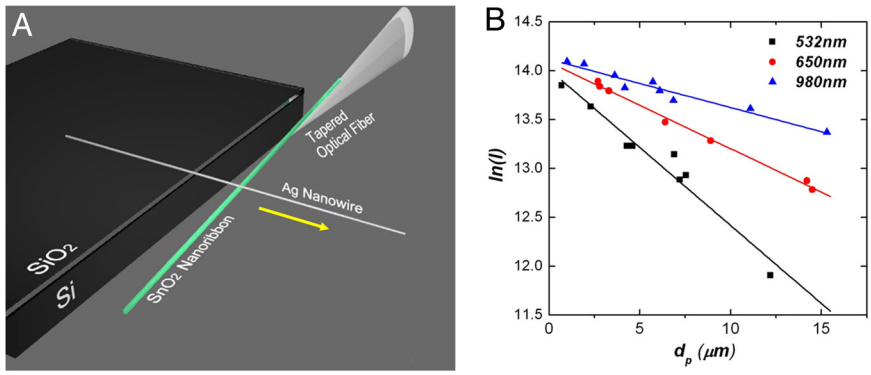

Fig. 3. Frequency dependence of Ag nanowire SPP propagation length (*L*). (*A*) Schematic representation of the experimental setup for measuring propagation length. A Ag nanowire is sitting on the edge of a thermal oxide substrate. Lasers of different frequencies were coupled into the Ag nanowire through a scanning SnO_2 nanoribbon probe attached to the end of an optical fiber. The yellow arrow indicates the sliding direction of the nanoribbon probe. (*B*) Plot of *ln*(*Intensity*) as a function of propagation distance d_p at two visible wavelengths: 532 (green) and 650 nm (red); and a NIR wavelength: 980 nm. The propagation lengths for the three wavelengths were 6.2, 11.3, and 20.2 μm, respectively.

into contact with a Ag nanowire sitting on the edge of an oxidized Si substrate.

Fig. 3*A* and Fig. S2 illustrate how this setup was used for the propagation length measurement. As the SnO_2-Ag junction was moved towards the tip of the Ag nanowire, the distance for which the SPP modes had to travel before scattering back into photons at the end-facet of the Ag nanowire (d_p) decreased, and the tip emission intensity (*I*) increased accordingly. If we assume that (*i*) the tip emission intensity was proportional to the intensity of the propagating SPPs modes, and (*ii*) the dielectric-metal (DM) coupling efficiency remains constant as the SnO_2 nanoribbon was sliding on the Ag nanowire, the only variable in the process was d_p. We can estimate in this way the propagation length (*L*) from the slope of the ln(*I*)- d_p plot. Here, it should be noted that our assumption of the constant coupling efficiency is based on the fact that the probe can glide along the perpendicular Ag nanowire without bending the wire, moving the coupling point on the probe or disturbing the coupling angle, as shown in Fig. S2 *b–f*.

Fig. 3*B* gives the typical ln(*I*)- d_p plots for three wavelengths: 532, 650, and 980 nm. The propagation length calculated from the slop of the plots shows strong frequency dependence, increasing from 6.2 μm (for 532 nm) to 11.3 μm (for 650 nm) and finally to 20.2 μm (for 980 nm) NIR excitation. And the SDs from different wires were <0.4 μm. Previous attempts to measure the propagation lengths in Ag nanowires through different approaches have set $L_{628\ nm}$ = 9.1 μm (16), $L_{785\ nm}$ = 10.1 ± 0.4 μm (5), and $L_{830\ nm}$ = 3 ± 1 μm (6), respectively. Although these results give reasonable estimations of the propagation lengths in their own systems and are in the same ballpark, they do not show a consistent trend and are hard to compare because of the different dielectric environments and measuring strategies in each case. Our measurement is a systematic demonstration of the frequency dependence of propagation lengths in Ag nanowires, which agrees well with the trend we observed in the case of broad-band excitation, as well as the result from fabricated Ag microstrips (21). The trend of increasing propagation length with wavelength extends to the telecommunication wavelength, according to the dispersion relation of the surface plasmon modes for a 100-nm metal cylinder in vacuum (22).

One important advantage of chemically-synthesized Ag nanowires, compared with fabricated nanowires, is the remarkably lower ohmic loss. The propagation length of a 1 μm wide, 70 nm high fabricated Ag microstripe on glass is <4 μm (21) at 633 nm (13 μm in numerical simulation) (23), ≈1/3 of a 100-nm diameter single crystalline Ag nanowire clad by air (11.3 μm), or sitting on a substrate (9.1 μm). Even for extended polycrystalline Ag films without lateral confinement, the propagation length of SPPs is 22 μm at 515 nm (20) and 60 μm at 633 nm (21), only four-five times larger than in our 100-nm Ag nanowires. This observation echoes in the theoretical simulation results for Ag nano-waveguides. Although direct simulation with completely air-clad Ag nanowire (as in our experiment) is still absent, numerical simulation based on Drude–Lorentz dispersion model set the propagation length for a 120-nm Ag nanowire sitting on a glass substrate at only 3.16 μm (24) at 785 nm when the Ag nanowire is considered as a low-crystallinity medium. However, when dealing with a single crystalline Ag nanowire, the increased electron mean free path due to absence of the crystalline domain walls has to be considered (25), and the modified model matches very well with the experimental data of synthesized Ag nanowire (10.1 ± 0.4 μm) (5). The low ohmic loss in these chemically synthesized nanowires arises from (*i*) the single crystalline nature, (*ii*) chemical homogeneity or low impurity level, and (*iii*) atomically smooth surfaces, all of which effectively reduce electron scattering during the collective oscillations in the metal.

The propagation length sets the upper size limit for any plasmonic feature on a photonic circuit. Another characteristic length, the decay length of electric field in surrounding dielectric environment, δ_d, which is typically on the order of half of the wavelength of light involved, dictates the maximum distance between any plasmonic or dielectric features that can have overlapping modes and couple to one another. Interwire coupling has been previous observed in a random assembly of Ag nanowires (6). However, a rational integration of dielectric and Ag nanowire waveguide components into optical-plasmonic routing devices, which is essential to incorporating Ag nanowire waveguides as practical components into highly-integrated photonic circuits, is yet to be demonstrated.

Here, both DM-metal (DMM) and DM-dielectric (DMD) coupling devices were designed and assembled to demonstrate the feasibility of optical-plasmonic routing. The device structure was illustrated in the SEM image in Fig. 4*A*, showing a silver nanowire sitting on top of a SnO_2 ribbon, with a second silver nanowire attached to it with a 12-μm overlap. The colored arrows points to the tips of the nanowires, and the magnified image of the Ag nanowire junction is given in the *Inset*. The surfactants on the Ag nanowires have been removed so that the two Ag nanowires were in direct contact. Fig. 4 *B* and *C* shows the intensity map and true-color image of the routing of SnO_2 ribbon PL. SPPs are launched into the first Ag nanowire at the metal (Ag)-dielectric (SnO_2) junction, and coupled into the second one evanescently without scattering loss along the metal-metal junction. They were scattered back into photons at the

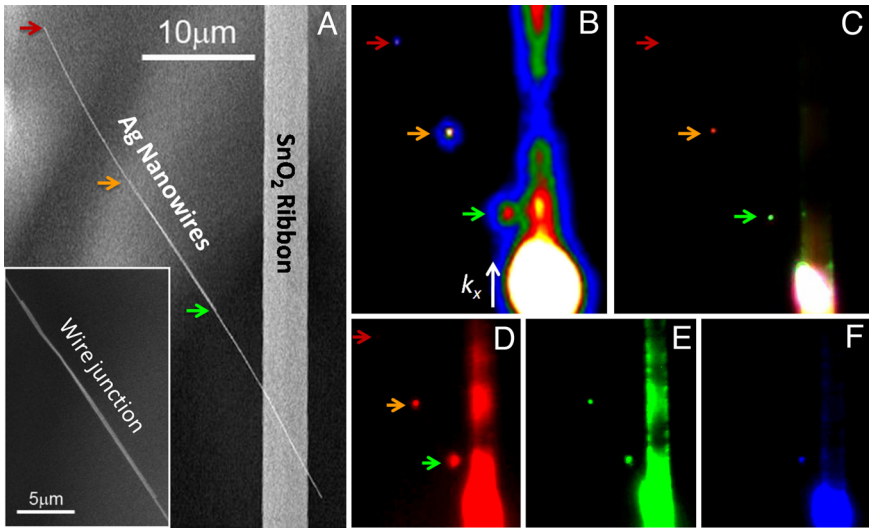

Fig. 4. DMM optical routing. (*A*) SEM image of the DMM routing structure, showing a pair of overlapping silver nanowires couple to a SnO_2 ribbon. The overlapping length of the two Ag nanowires was 12 μm. (*Inset*) Overlapping section of the two metal nanowires. The end of Ag nanowire-1 was marked by the orange arrow. The tips of Ag nanowire-2, which was not in direct contact with the ribbon were marked with the green and red arrows. (*B*) Intensity map of the routing device when the PL of the SnO_2 ribbon was excited from far below (out of scope) and coupled into nanowire-1 that is in direct contact with the ribbon and then propagate to nanowire-2, showing three distinct emission points at the three distal ends of the nanowires. (*C*) The true-color image of the same view as in *B*. (*D–F*) Single R (red), G (green), and B (blue) color channels from *C*, showing a systematic decrease in propagation loss from blue to red optical frequencies. The colors are from the Bayer filter in the CCD image sensor (Sony ICX 205AK) of the CoolSnap cf camera.

three discontinuities (wire tips) along the propagation direction, as marked by the color arrows whose positions are in accordance with Fig. 4*A*. Despite the radiative losses at the wire tips, the SPP modes are able to propagate without complete attenuation to the farthest tip of the second wire that was 40 μm away from the excitation (Ag-SnO_2 junction). This efficient plasmonic coupling between Ag nanowires in this routing device was a comprehensive result of the overlapping k_x, the long Ag-Ag junction, and the large SPP mode overlapping due to the minimum distance between the wires.

It should be noted that the dependence of the tip emission color on d_p in the single nanowire case is also observed in the coupling device. Fig. 4 *D* and *F* displays the red, green, and blue color panel of the true-color image in Fig. 4*C*. The closer the tips were to the excitation, their emissions composed more high-frequency components. The blue components only exist at the first Ag nanowire tip that is 8 μm from the excitation, whereas green ones survived 20 μm of propagation, and the red ones were the only visible frequencies that were observable at farthest emission point, 40 μm from excitation.

The design of the DMD coupling device is shown in the dark-field microscope image (Fig. 5*A*). The two SnO_2 nanoribbons lying on an oxidized Si substrate were bridged with an Ag nanowire. The PL of the bent ribbon was excited from hundreds of micrometers away from the Ag-SnO_2 junctions to avoid direct excitation of the straight ribbon. In the absence of the Ag nanowire (Fig. 5*B*), the propagating modes of the straight ribbon was not excited, with only a week scattering signal at the tip close to the bent ribbon. However, with the Ag nanowire bridging the two ribbons, the SPPs launched into the Ag nanowire couple back to guided optical modes in the straight ribbon, which then propagate 43 μm to the distal end and scatter into free-space photons.

In conclusion, we have demonstrated the coupling between photonic and plasmonic waveguides at the single nanowire level. The frequency-dependent propagation loss was observed in Ag nanowire and was confirmed by quantitative measurement and in agreement with theoretical expectations. Rational integration of dielectric and Ag nanowire waveguide components into hybrid optical-plasmonic routing devices has been demonstrated. This capability is essential for incorporating low-loss Ag nanowire waveguides as practical components into high-capacity photonic circuits and can be extended to other inorganic dielectric waveguide systems such as Si, SiO_2, GaN, and Si_3N_4.

Materials and Methods

SnO_2 Nanoribbon Synthesis. SnO_2 nanoribbon waveguides were synthesized using a chemical vapor transport method previously described (26). SnO

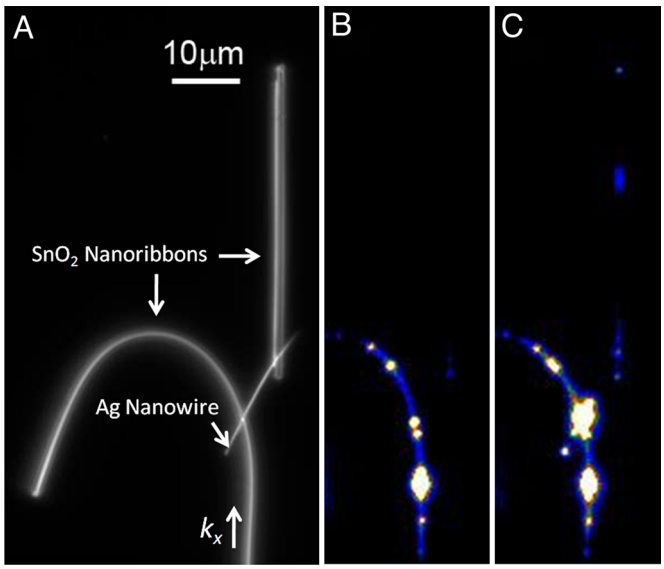

Fig. 5. DMD optical routing circuit. (*A*) Dark field optical image of the DMD coupling device, showing two SnO_2 nanoribbon bridged by a silver nanowire. (*B*) Optical image of the intensity map of the device in the absence of the bridging Ag nanowire when the PL of the bent SnO_2 nanoribbon was excited from the bottom end (excitation spot not shown). No signal from the vertical ribbon was observed. (*C*) Optical image of the intensity map of the device with the bridging Ag nanowire, showing a significant increase in the optical field in the vertical ribbon.

powder was heated in a quartz tube reactor at 1,100 °C under 350 Torr of flowing argon (50 sccm). Milligram quantities of ribbons were collected on an alumina boat near the center of the reactor and deposited onto clean substrates by dry transfer.

Ag Nanowire Synthesis. The Ag nanowires were synthesized by reducing $AgNO_3$ with ethylene glycol (EG) in the presence of Polyvinylpyrrolidone (PVP) (27). Three stock solutions for the Ag nanowire synthesis were prepared at room temperature by dissolving 50 mg NaCl, 50 mg $AgNO_3$, and 200 mg PVP (50,000 g/mol) in 20 mL EG, respectively; 50 μL $AgNO_3$ solution and 150 μL NaCl solution was added to 5 mL of PVP solution while stirring at room temperature in a 25 mL flask. After 5 min, the flask was then transferred to an oil bath at 170–180 °C, heated for ≈5 min until the mixture turned from white to orange, and injected with additional 0.5–2 mL of $AgNO_3$. After heating for 10–15 more minutes, the product was collected and washed with EG and ethanol to remove excess PVP. The purified nanowires were stored in ethanol. The product was then drop-cast on a PDMS substrate for manipulation. The synthesis yield large quantity of nearly pure Ag nanowires with nearly monodispersed diameter (100 nm) and lengths up to 50 μm.

Optical Characterization. A HeCd laser (Melles Griot) provided unpolarized continuous wave (CW) UV excitation (325 nm) for the PL of SnO_2 waveguide. CW diode lasers (532, 650, and 980 nm) supplied visible lights for the propagation length measurement. The lasers were either focused to a beam diameter of 50 μm on the SnO_2 nanoribbons or coupled to an optical fiber.

Intensity maps and color images were recorded with two microscope-mounted cameras (iXon, Andor Technology, and CoolSnap cf, Photometrics). The tip-emission spectra measurement was performed with an inverted microscope (IX71, Olympus). Signal was collected through a 60× microscope objective lens (NA = 0.7) and captured by a 1,340 × 400 pixel, back-illuminated CCD (Spec-10:400B, Princeton Instruments) and spectrometer (SpectraPro 2300i, Princeton Instruments).

Manipulation and Probe Fabrication for the Propagation Length Measurement. For nanoribbon manipulation, we used a three-axis commercial micromanipulator equipped with tungsten probes (≈400-nm tip diameter). The probe used for exciting the ribbon waveguide was fabricated by attaching a SnO_2 nanoribbon to a chemically-etched (28) multimode UV-IR optical fiber with epoxy adhesive.

ACKNOWLEDGMENTS. This work was supported by the Director, Office of Science, Office of Basic Energy Sciences, Division of Materials Sciences and Engineering of the Department of Energy under Contract DE-AC02-05CH11231, and by the National Institutes of Health.

1. Lal S, Link S, Halas NJ (2007) Nano-optics from sensing to waveguiding. *Nat Photonics* 1:641–648.
2. Ozbay E (2006) Plasmonics: Merging photonics and electronics at nanoscale dimensions. *Science* 311:189–193.
3. Barnes WL, Dereux A, Ebbesen TW (2003) Surface plasmon subwavelength optics. *Nature* 424:824–830.
4. Graff A, Wagner D, Ditlbacher H, Kreibig U (2005) Silver nanowires. *Eur Phys J D* 34:263–269.
5. Ditlbacher H, et al. (2005) Silver nanowires as surface plasmon resonators. *Phys Rev Lett* 95:257403.
6. Sanders AW, et al. (2006) Observation of plasmon propagation, redirection, and fan-out in silver nanowires. *Nano Lett* 6:1822–1826.
7. Krenn JR, Weeber JC (2004) Surface plasmon polaritons in metal stripes and wires. *Philos T Roy Soc A* 362:739–756.
8. Maier SA (2006) Plasmonics: The promise of highly integrated optical devices. *Ieee J Sel Top Quant* 12:1671–1677.
9. Maier SA, et al. (2003) Local detection of electromagnetic energy transport below the diffraction limit in metal nanoparticle plasmon waveguides. *Nat Mater* 2:229–232.
10. Krenn JR, et al. (2002) Non diffraction-limited light transport by gold nanowires. *Europhys Lett* 60:663–669.
11. Zia R, Schuller JA, Brongersma ML (2006) Near-field characterization of guided polariton propagation and cutoff in surface plasmon waveguides. *Phys Rev B* 74:165415.
12. Dickson RM, Lyon LA (2000) Unidirectional plasmon propagation in metallic nanowires. *J Phys Chem B* 104:6095–6098.
13. Knight MW, et al. (2007) Nanoparticle-mediated coupling of light into a nanowire. *Nano Lett* 7:2346–2350.
14. Fedutik Y, Temnov V, Woggon U, Ustinovich E, Artemyev M (2007) Exciton-plasmon interaction in a composite metal-insulator-semiconductor nanowire system. *J Am Chem Soc* 129:14939–14945.
15. Akimov AV, et al. (2007) Generation of single optical plasmons in metallic nanowires coupled to quantum dots. *Nature* 450:402–406.
16. Pyayt AL, Wiley B, Xia Y, Chen A, Dalton L (2008) Integration of photonic and silver nanowire plasmonic waveguides. *Nat Nanotechnol* 3:660–665.
17. Law M, et al. (2004) Nanoribbon waveguides for subwavelength photonics integration. *Science* 305:1269–1273.
18. Sirbuly DJ, et al. (2005) Optical routing and sensing with nanowire assemblies. *Proc Natl Acad Sci USA* 102:7800–7805.
19. Sirbuly DJ, Law M, Yan HQ, Yang PD (2005) Semiconductor nanowires for subwavelength photonics integration. *J Phys Chem B* 109:15190–15213.
20. Raether H (1988) *Surface Plasmons on Smooth and Rough Surfaces and on Gratings* (Springer, Berlin).
21. Lamprecht B, et al. (2001) Surface plasmon propagation in microscale metal stripes. *Appl Phys Lett* 79:51–53.
22. Novotny L, Hafner C (1994) Light-Propagation in a Cylindrical Wave-Guide with a Complex, Metallic, Dielectric Function. *Phys Rev E* 50:4094–4106.
23. Zia R, Selker MD, Brongersma ML (2005) Leaky and bound modes of surface plasmon waveguides. *Phys Rev B* 71:165431.
24. Laroche T, Girard C (2006) Near-field optical properties of single plasmonic nanowires. *Appl Phys Lett* 89:233119.
25. Laroche T, Vial A, Roussey M (2007) Crystalline structure's influence on the near-field optical properties of single plasmonic nanowires. *Appl Phys Lett* 91:123101.
26. Pan ZW, Dai ZR, Wang ZL (2001) Nanobelts of semiconducting oxides. *Science* 291:1947–1949.
27. Sun YG, Yin YD, Mayers BT, Herricks T, Xia YN (2002) Uniform silver nanowires synthesis by reducing AgNO3 with ethylene glycol in the presence of seeds and poly(vinyl pyrrolidone). *Chem Mater* 14:4736–4745.
28. Haber LH, Schaller RD, Johnson JC, Saykally RJ (2004) Shape control of near-field probes using dynamic meniscus etching. *J Microsc-Oxford* 214:27–35.